Synchronized Measurement Technology Supported Online Generator Slow Coherency Identification and Adaptive Tracking

Naglic, Matija; Popov, Marjan; van der Meijden, Mart A.M.M.; Terzija, Vladimir

DOI
10.1109/TSG.2019.2962246

Publication date
2020

Document Version
Final published version

Published in
IEEE Transactions on Smart Grid

Synchronized Measurement Technology Supported Online Generator Slow Coherency Identification and Adaptive Tracking

Matija Naglic, *Student Member, IEEE*, Marjan Popov, *Senior Member, IEEE*, Mart A. M. M. van der Meijden, *Member, IEEE*, and Vladimir Terzija, *Fellow, IEEE*

***Abstract*—In an electric power system, slow coherency can be applied to identify groups of the generating units, the rotors of which are swinging together against each other at approximately the same oscillatory frequencies of inter-area modes. This serves as a prerequisite-step of several emergency control schemes to identify power system control areas and improve transient stability. In this paper, slow coherent generators are grouped based on the direction and the strength of electromechanical coupling between different generators. The proposed algorithm performs low-pass filtering of generator frequency measurements. It adaptively determines the minimal number of the measurements to be processed in an observation window, and performs data selectivity to prevent mixing of interfering coherency indices. Finally, it adaptively tracks grouping changes of slow coherent generators and determines a finite number of groups for an improved affinity propagation clustering. The proposed algorithm is implemented as an online MATLAB program and verified in real-time using RTDS power system simulator with the integration of actual synchronized measurement technology components as hardware-in-the-loop. The obtained results demonstrate the effectiveness of the proposed algorithm for robust and near real-time identification of grouping changes of slow coherent generators during the quasi-steady-state and electromechanical transient period following a disturbance.**

***Index Terms*—Coherent detection, clustering algorithms, real-time systems, wide area measurements.**

I. Introduction

EMERGING renewable energy sources, decreased system inertia, and economic reasons have forced electric power systems to operate closer to their stability limits [1]. Unexpected disturbances, component failures, or human errors may cause large-scale power system emergencies, leading to a catastrophic system-wide blackout [2].

To mitigate such extreme events and improve system reliability, the Synchronized Measurement Technology (SMT) supported System Integrity Protection Schemes (SIPS) have been developed. The purpose of SIPS is to detect immediate critical instabilities, arrest the disturbance propagation, and restore the system to stable operation with minimal consequences [3]. Typically, supported by a global navigation satellite system, the SMT makes use of Phasor Measurement Units (PMUs) to deliver time-synchronized measurements (synchro-measurements) from remote locations in near real-time [4]. SMT is of the key element of Wide Area Monitoring, Protection and Control (WAMPAC) system [5], to which the SIPS belong [6]. In order to increase the effectiveness of emergency control on system stability, especially in case of an intentional controlled islanding (ICI) [7], [8], [9] and wide-area oscillation damping [10], the generator slow coherency is often a required constraint. Besides, the generator slow coherency is used for a dynamic equivalencing to reduce a power system model size and complexity [11], [12].

A. Generator Slow Coherency

In an electric power system, generators are said to be coherent if their rotor angles undergo similar time-domain response [11], [12]. Slow coherent generator groups, i.e., generators swinging together at oscillatory frequencies of the inter-area modes (0.1 to 0.8 Hz), have a relatively strong electromechanical coupling [8], [12], [13]. In this work, the low-pass filtering of measurements is performed to retain only the inter-area modes of interest and enable grouping of slow coherent generators during the quasi-steady-state and the electromechanical transient period following a disturbance.

The slow coherent generators have a high tendency to operate synchronously, even after being exposed to the severe network perturbation following a disturbance such as a fault [12]. Nevertheless, the generators may change their coherent groups as a response on the modified system state following a significant disturbance such as topology change, generator trip, or large load step [9]. Therefore, the ability to online track the slow coherent behavior of generators in a disturbed power system in real-time is a relevant challenge. Singh *et al.* discuss the commonly used coherency methods for

Manuscript received March 15, 2019; revised June 21, 2019, September 18, 2019, and November 6, 2019; accepted December 12, 2019. Date of publication December 25, 2019; date of current version June 19, 2020. This work was supported in part by the Dutch Scientific Council NWO in collaboration with TSO TenneT, DSOs Alliander, Stedin, and Enduris, and in part by the General Electric in the Framework of the Energy System Integration and Big Data Program under the Project “Resilient Synchromeasurement-Based Grid Protection Platform” under Grant 647.003.004. Paper no. TSG-00386-2019. *(Corresponding author: Matija Naglic.)*

Matija Naglic and Marjan Popov are with the Faculty of Electrical Engineering, Mathematics, and Computer Science, Delft University of Technology, 2628 CD Delft, The Netherlands.

Mart A. M. M. van der Meijden is with the Faculty of Electrical Engineering, Mathematics, and Computer Science, Delft University of Technology, 2628 CD Delft, The Netherlands, and also with TenneT TSO, 6812 AR Arnhem, The Netherlands.

Vladimir Terzija is with the School of Electrical and Electronic Engineering, University of Manchester, Manchester M139PL, U.K.

Color versions of one or more of the figures in this article are available online at http://ieeexplore.ieee.org.

Digital Object Identifier 10.1109/TSG.2019.2962246

aggregation of generators [14]. These methods firstly assess generator coupling indices being further used for clustering of coherent generators into groups.

The classical approach to identify slow coherent generator groups belongs to model-based methods [7], [12]. These methods perform the eigensubspace analysis of a linearized power system model. The resulting analysis is valid only for a particular equilibrium point and suffers from the modeling inaccuracies and parametric uncertainties. While being able to provide valuable information about the general dynamic structure of the power system, the slow coherency theory does not consider the transient dynamics of the system. However, during the power system contingency operation, the swings of generators with respect to each other are influenced not only by the structure of the system, but also by the type and location of the disturbance, generator internal electrical dynamics, and controller's response [15]. Any significant change in the power system operating state, such as a topology change, large load step, or generator trip, might cause the weakly slow coherent generators to change their grouping association [16]. This makes the model-based methods not suitable for online use in actual power systems [17]. Therefore, the ability to track the slow coherent behavior of generators in a profoundly disturbed power network in real-time is a relevant problem that cannot be directly solved by the model-based methods.

In order to overcome the abovementioned deficiencies, measurement-based methods have been developed. Their main advantage is the inherent ability to adapt and online identify the grouping changes of slow coherent generators following a contingency, as well as in independence from the system parameter data. Those methods can be coarsely sub-classified into mode estimation analysis, and time-series similarity-based techniques. The methods belonging to the first sub-class estimate the system modes or frequency spectrum and partition the coherent generators into groups by using k-means, fuzzy and agglomerative hierarchical clustering algorithm [18]–[22]. While being able to extract information about the inter-area oscillations, these techniques often suffer from the mode estimation related inaccuracies, and high processing power required to process the relatively long observation window. Therefore, mode estimation methods are most suitable for offline analysis. On the other hand, the time-series similarity-based methods identify generator coherency based on the similarities of the extracted features (indices), typically with less processing power required [14], [15], [16]. Generally, these methods are most suitable for online operation but suffer from the inability to operate only on the frequency content of interest (inter-area oscillations). A data mining-based technique [23] has been presented to identify the unstable system operation and identify coherent generators based on the supervised offline training of binary classifiers. Despite the fast and high accuracy of estimates, this method suffers from an inherent requirement to perform a substantial number of model-based supervised training simulations making this method suitable only for a limited set of disturbances and well-detailed power system models. Recently, a spectral clustering based method was presented, which makes use of generator rotor angle and speed measurements to assess the weighted multi-indices dissimilarity distance [24]. The optimal number of coherent groups is determined by comparing the average silhouette value of different clustering combinations (number of groups), and finally selecting the clustering configuration with the highest average silhouette value among all evaluated cases. However, limited availability of the rotor angle and speed measurements makes the implementation of this moment not applicable in real-world power systems. The method presented in [25] makes use of kernel principal component analysis and affinity propagation (AP) clustering technique to reduce dimensions of the multi-indices distances and to automatically determine the optimal number of coherent groups. However, this method also requires center-of-inertia centered generator rotor angles and speeds; and due to the basic preference parameter method for the AP clustering tends to partition independent (outlier) generators to the nearest group, leading to suboptimal results. Authors in [15] presented the dynamic coherency identification method suitable for online tracking of coherent generator grouping changes based on the PMU measured frequency-deviation from the generator terminals. This method also partitions the non-generator buses together with the corresponding coherent generator groups. The authors further extend the method in [26] to consider also the transient behavior of wind power plants. The work, presented in [15], tends to tackle the same challenge as the proposed algorithm of this paper, in particular to online identify grouping changes of coherent generators following a disturbance for the purpose of ICI. Therefore, the method presented in [15] (referred further as the benchmark method) is used in this paper for a comparison analysis.

B. Paper Motivations and Contributions

The available measurement-based generator coherency identification methods, in particular, the benchmark method, {i} do not preprocess the measurements to retain only inter-area oscillation frequencies of interest, {ii} require relatively long and non-adaptive observation window, {iii} do not perform observation window data selectivity for vigorous coherency identification in case of interfering pre- and post-event coherency indices, {iv} and are validated upon conventional software simulated bus measurements rather than actual PMU synchro-measurements. These deficiencies may lead to {i} erroneous results, {ii} impose large identification delay, and poor resolution of estimates after critical disturbances.

This paper addresses the abovementioned deficiencies and proposes a novel SMT supported online generator slow coherency identification algorithm, suitable for near real-time tracking of grouping changes of slow coherent generators following a contingency. The main contributions of this paper include the following:

1. Improved generator dissimilarity measure method to thoroughly assess generator coherency indices as a direction and strength of electromechanical coupling.
2. Novel observation window length method to adaptively determine the minimum number of processed samples.
3. Novel data selectivity method to prevent mixing of the interfering pre- and post-event coherency indices within a given observation window following a contingency.

4. Novel adaptive tracking method of grouping changes of the slow coherent generators during a quasi-steady-state and electromechanical transient period.
5. New preference adjustment method of the affinity propagation clustering to identify outlier generators and define a finite number of coherent groups adaptively.

C. Paper Organization

The rest of the paper is organized as follows: Section II addresses the relevant challenges and describes the proposed algorithm. Section III presents the simulation platform, being used for online evaluation and comparison. Sections IV and V present and discuss the obtained results, respectively. Finally, Section VI concludes this paper and addresses future work.

II. Proposed Methodology

In the previous section, a formal introduction to the generator slow coherency identification is provided. However, the practical implementation of the generator slow coherency identification for online use has revealed several new and unresolved challenges. Herein, we address the identified ones and present the proposed solutions.

A. Data Selection

Generally, the generator rotor angle provides the most direct information about the rotor dynamics and related generator coherency [13]. However, PMU devices do not report rotor angle measurements, and even rotor angle estimations based on PMU voltage angle measurements may produce inaccurate results. As suggested in [12], [15], [27] a PMU, installed at the generator terminal bus, can send frequency measurements of positive sequence voltage containing vague information of the rotor associated dynamics. Hence, a PMU device can be used to monitor interarea oscillations of interest of the particular generator in a power system (further discussed in Section II-B).

It is assumed that in an electric power system consisting of N generators, each generator terminal bus is equipped with a PMU device. Each PMU device $i \in \{1, 2, \ldots, N\}$ reports discrete time-interval samples of terminal frequency x with 60 frames per second reporting interval (hereinafter referred to as *fps*). With M being the total number of samples to be processed, the sample vector is defined as $X_i = [x_{i,M}, \ldots, x_{i,2}, x_{i,1}] \in R^{1\times M}$, where $x_{i,1}$ denotes to the most recent frequency measurement of PMU i. The observation window W, containing M-most recent samples of frequency from N generator terminal buses, is presented by the following ensembled matrix:

$$\mathrm{W[X]} = \begin{bmatrix} \mathrm{X}_1 \\ \mathrm{X}_2 \\ \vdots \\ \mathrm{X}_\mathrm{N} \end{bmatrix} = \begin{bmatrix} \mathrm{x}_{1,\mathrm{M}} & \cdots & \mathrm{x}_{1,2} & \mathrm{x}_{1,1} \\ \mathrm{x}_{2,\mathrm{M}} & \cdots & \mathrm{x}_{2,2} & \mathrm{x}_{2,1} \\ \vdots & \ddots & \vdots & \vdots \\ \mathrm{x}_{\mathrm{N},\mathrm{M}} & \cdots & \mathrm{x}_{\mathrm{N},2} & \mathrm{x}_{\mathrm{N},1} \end{bmatrix} \in \mathrm{R}^{\mathrm{N}\times\mathrm{M}}. \tag{1}$$

B. Data Preprocessing

Generator slow coherency is defined upon inter-area oscillation modes typically between 0.1 to 0.8 Hz, which are associated with the rotor swings between a group of generators or plants [12], [13]. Any higher frequency components present in the PMU measurements, as a consequence of excited local plant oscillations, may result in erroneous generator slow coherency identification [28]. Moreover, actual PMU measurements are affected by transients, and system imposed high-frequency components such as measurement noise [29]. Therefore, for generator slow coherency identification, it is prudent to preprocess the measurements in order to retain only the inter-area oscillation frequencies of interest. Despite the evident interest of the research community for measurement-based generator coherency identification, only a small number of papers [22], [30] address the issue of high-frequency components present in the measurements. In this paper, only the most critical low-pass filtering and down-sampling are addressed.

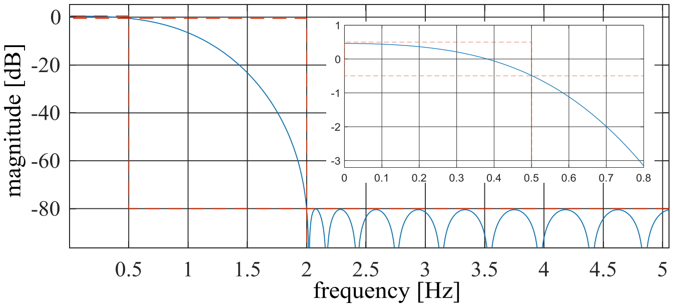

Fig. 1. Magnitude response of the digital low-pass FIR filter for 60 fps.

TABLE I
FIR Filter Parameters

design algorithm:	Equiripple	passband ripple:	1 dB
filter length:	126 samples	stopband edge:	2 Hz
filter delay:	63 samples	passband edge:	0.5 Hz
response:	low-pass	stopband attenuation:	80 dB

1) Digital Low-Pass Filtering: Digital filtering is extensively adopted in many diverse applications to perform frequency-dependent alteration of an original signal. It can be used for noise reduction and frequency band extraction. In this paper, a low-pass finite-duration impulse response (FIR) filter is adapted due to its filtering superiorities [31]. The design of a low-pass FIR filter with a narrow frequency band between 0 to 0.8 Hz and sharp cut-off slope requires a relatively long filter order (length) to sufficiently suppress higher frequency components. Fig. 1 and Table I present the used filter response and design parameters, respectively.

It is important to note that digital filtering introduces unavoidable delay since the filter output samples are shifted in time compared to the input. During the initialization period, the filter is loaded with zeros, which causes transients in the output until the filter is fully loaded with actual measurements. Thus, during the filter initialization period, it is prudent to discard the number of output samples equal to the filter length.

2) Downsampling: As suggested in [30], a typical PMU 50/60 fps rate provides measurements significantly faster compared to the electromechanical modes of interest resulting in redundant information. In this paper, 60 fps PMU reporting rate is selected. However, the preformed simulations (not part of this paper) confirm that the proposed algorithm performance is not affected in case of used 10, 15, and 30 fps PMU reporting rate.

C. Generator Distance Matrix

For generator coherency identification, a distance matrix $DM \in R^{N\times N}$ is used to define relations between the pairs of generators, where DM_{mn} denotes the dissimilarity between the m^{th} and n^{th} generator. To determine the *DM*, as presented in [32], a wide variety of distance measures can be used, in particular, to assess the generators' slow coherency indices.

In this paper, a revised generator dissimilarity measure method of the benchmark method is proposed to assess the coherency indices in greater detail. This is realized as a weighted combination of the normalized *cosine* and *Minkowski p*-metric based distance matrices. Cosine distance measure determines an angular displacement, whereas the Minkowski distance measure determines a modified Euclidean norm between a set of sample vectors *X*, embedded in *M*-dimensional vector space [33]. The $dcos_{mn}[X]$ between two sample vectors *X* with *M*-dimensional points of generator *m* and *n* is defined as:

$$\mathrm{dcos_{mn}[X]} := 1 - \frac{\sum_{k=1}^{M} \mathrm{X_{m,k}X_{n,k}}}{\sqrt{\sum_{k=1}^{M} \mathrm{X_{m,k}}^2}\sqrt{\sum_{k=1}^{M} \mathrm{X_{n,k}}^2}} \in \mathrm{R}^{1\times 1} \quad (2)$$

and ranges from 0 to 2, where 0 indicates perfect angular alignment. Similarly, the $dmik_{mn}[X]$ of order $b = 1/2$ between two sample vectors *X* with *M*-dimensional points of generator *m* and *n* is defined as:

$$\mathrm{dmik_{mn}[X]} := \left(\sum_{k=1}^{M} \left|\mathrm{X_{m,k}} - \mathrm{X_{n,k}}\right|^{\mathrm{b}}\right)^{1/\mathrm{b}} \in \mathrm{R}^{1\times 1} \quad (3)$$

and ranges from 0 to 8, where 0 indicates perfect magnitude match. The proposed distance matrix method represents a weighted combination of the normalized cosine $DMcos[X] \in R^{N\times N}$ and Minkowski $DMmik[X] \in R^{N\times N}$ symmetric distance matrixes to assess the orientation and strength of generators electromechanical coupling, respectively. To reduce the required memory and computational power both distance matrices, named as $DM \in R^{N\times N}$, are converted into a row distance vectors $DV \in R^{1\times L}$ of length $L = (N-1)N/2$, where between the generator pair distances are arranged as:

$$\mathrm{DV} = \left[\mathrm{DM_{1,2}}, \ldots, \mathrm{DM_{1,N}}, \mathrm{DM_{2,3}}, \ldots, \mathrm{DM_{2,N}}, \ldots, \mathrm{DM_{N-1,N}}\right] \in \mathrm{R}^{1\times \mathrm{L}} \quad (4)$$

To ensemble both distance vectors into a single vector a unit vector normalization is performed beforehand as:

$$\mathrm{DVN} := \frac{\mathrm{DV}}{\sqrt{\sum_{k=1}^{L} \mathrm{DV}^2}} \in \mathrm{R}^{1\times \mathrm{L}} \quad (5)$$

Finally, the generator distance vector $DVG \in R^{1\times L}$ to be used resembles the *Euclidean norm* of the weighted individual dissimilarities, where the vectors' elements are represented as scalars in 2-dimensional Euclidean space by the equation:

$$\mathrm{DVG[t]} := \sqrt{\mathrm{w_1\{DVNcos[X]\}^2 + w_2\{DVNmik[X]\}^2}} \in \mathrm{R}^{1\times \mathrm{L}} \quad (6)$$

where $w_1 = 1$, $w_2 = 0.5$ represent the heuristically determined contributions of individual measures; and $t \in \{1, 2, \ldots\}$ resembles the time index as a point in time of a given variable. In this way, the angular displacement (cosine distance) impacts the results more significantly, although the identification of areas with different frequency (Minkovski distance) is still possible.

D. Adaptive Observation Window

The existing generator coherency identification methods expect a long (10 - 20 *s*) and a non-adaptive (fixed in length) observation window. While this approach mostly works well during quasi-steady-state, it lacks fast response and resolution during the critical electromechanical transient period following a contingency. Generally, the stronger the power system is perturbed, the more conspicuous the present generator coherency is. In other words, one could online adjust the observation window length based on the present system state. In this paper, the observation window length *M* is automatically adjusted for each coherency identification instance. In general, the shorter the observation window, the more sensitive is the algorithm to temporary coherency changes. However, a too short window may lead to irrational results due to the lack of observability. Also, the window length decrease is proportionally related to the decrease in identification latency and computational power.

The proposed adaptive observation window length method is based on a stability criterion, driven by the angular deviation of two most recent successive generator distance vectors (6) in *L*-dimensional vector space, as illustrated in Fig. 4 - bottom. The following procedure determines the minimum number of samples to be processed for rigorous coherency identification:

a. Initialization: set the window length to $M = fps$ to provide minimum observability, fix the observation window starting position (remains fixed till *Exit*) to the first incoming measurement sample being low-pass filtered, populate the observation window with *M* consecutive samples, determine the normalized generator distance vector $DVG[t]$ (2) - (6), and save $DVG[t]$ for later use.

b. Increase the window length as $M = M + 1$, and populate the observation window with a next-measurement-interval sample. Again determine the $DVG[t]$ and save it for later use.

c. Determine the *cosine* angular difference $\Delta DVG[t]$ between the two most recent consecutive *DVG* vectors in *L*-dimensional vector space by using equations (2) and (7) and save it for later use as:

$$\Delta\mathrm{DVG[t]} := \cos^{-1}\left\{\mathrm{dcos_{t-1,t}(DVG)}\right\} \quad (7)$$

d. Exit condition: if the median of $(fps/5 + 1)$ most recent angular deviations ΔDVG (7) drops below the heuristically determined threshold $stab\_tresh = 3/fps$, as:

$$\mathrm{median}\left\{\Delta\mathrm{DVG}\left[\mathrm{t} - (\mathrm{fps}/5)\right] \cdots \Delta\mathrm{DVG[t]}\right\} \leq \mathrm{stab\_tresh} \quad (8)$$

then the current window length adjustment procedure finishes (see Fig. 4 - bottom) and continues with the data selectivity method (Section II-E). In this case, the next observation window for next coherency identification instance starts with the next incoming sample of step *a*. Otherwise, the procedure continues with step *b* and so forth.

Notably, *stab_tresh* plays a vital role in determining the observation window length. The performed simulations suggest that it can typically range between $0.01 \geq$ *stab_tresh* ≥ 0.1, where a smaller value leads to a shorter observation window (higher resolution of estimates; more sensitive to temporal changes), whereas a higher value indicates a longer observation window (lower resolution of estimates; more robust to temporal changes). In our case, the *stab_tresh* is controlled by the PMU reporting rate automatically.

E. Reverse Data Selectivity

During the electromechanical transient period following a significant disturbance, such as a line trip, the generator coherency may change. This can be observed in the change of coherency indices. In this case, the observation window containing interfering pre- and post-event coherency indices (measurements) may result in erroneous coherency identification. Especially during critical post-event period, it is prudent to perform data selectivity on the given observation window to prevent mixing of the interfering indices and retain only the observation window measurements belonging to the post-event. The following steps significantly improve the critical coherency results immediately after an event:

e. Initialization: flip the order of elements of the observation window W, named as $W_{flipped}$. This enables processing of $W_{flipped}$ elements in a reverse direction to retain only the post-event samples; set the minimum observation window length $M_{flipped} = fps$.

f. In steps for each increase in $M_{flipped}$ repeat Section II-D steps *a, b, c* (mind to use (2) - (7) with $W_{flipped}[1{:}M_{flipped}]$).

g. Exit condition: a severe change in coherency indices is detected if the following selectivity threshold condition (mind the red line in Fig. 7 - bottom) is satisfied:

$$\Delta \mathrm{DVG_{flipped}[t]} \geq 60\, \mathrm{M_{flipped}}^{-(\mathrm{fps}/300+0.6)} \tag{9}$$

Afterward, a local minima search is performed on the $\Delta DVG_{flipped}$, to identify the instant when the $\Delta DVG_{flipped}$ elements start to deviate, indicating a change in coherency indices. This step tends to find the last dip $\Delta DVG_{flipped}[local\_min]$ (for example, mind the blue circle in Fig. 7 - bottom). The procedure continues with Section II-F, where the *DVG* to be further used in Section II-F is equal to the $DVG_{flipped}[local\_min]$.

h. In case the condition in step *g* is not satisfied, indicating sustained coherency indices within the given observation window, then the *DVG* to be used in Section II-F is identical to the last determined *DVG*[*t*] of Section II-D.

F. Adaptive Tracking

Generator slow coherency is a quasi-permanent system property under sustained system state. During a severe disturbance, such as the topology change, the generator slow coherency may change as a response of the generators on the new operating state. To enable adaptive tracking of grouping changes of slow coherent generators, two operation modes are proposed. A *permanent mode* is activated during the quasi-steady-state, while a *transient mode* is activated during the electromechanical transient period following a significant disturbance. In both cases the first-order exponential low-pass filter is adopted to enable robust coherency identification, being prone to temporally changes in a power system state, caused by transients due to small load changes, for example.

1) Permanent Tracking Mode: Typically, during quasi-steady-state, the generator coherency does not change significantly. However, it may happen that due to temporal small system perturbations the weakly coherent generators separate and form new groups. To enable robust generator coherency identification meanwhile being still able to adapt to the grouping changes, the *DVGA*[*t*] (10) vector to be used as an input for the AP clustering (see Section II-G) resembles the proportional contribution of the most recent *DVG*[*t*] (6) and *DVGA*[$t-1$], defined in the previous coherency estimation instance, as:

$$\mathrm{DVGA[t]} := \alpha \mathrm{DVGA[t-1]} + (1-\alpha)\mathrm{DVG[t]} \tag{10}$$

where heuristically determined $\alpha = 0.7$ controls contributions of the previously determined coherency indices *DVGA*[$t-1$].

Generally, α can range between 0 and 1, where a higher value of α puts more weight on the past coherency indices leading to more robust results, while on the contrary, a smaller value of α leads to increased adaptiveness of the algorithm to the most recent coherency indices of *DVG*[*t*].

2) Transient Tracking Mode: On the other hand, to enable more responsive tracking of grouping changes of slow coherent generators during the critical electromechanical transient period, when the slow coherency may change, the *DVGA*[*t*] to be used is next step (mind Section II-G) is defined as (10), where $\alpha = 0.4$ enables better adaptiveness to the present coherency configuration.

3) The Transition Between the Tracking Modes: The transition between the tracking modes is based on a cosine angular difference of the two most recent *DVGA* vectors defined as:

$$\Delta \mathrm{DVGA[t]} := \cos^{-1}\left\{\mathrm{dcos_{t-1,t}(DVGA)}\right\} \tag{11}$$

A significant increase in $\Delta DVGA[t]$ indicates a significant change in the generator coherency indices, while minor changes indicate sustained conditions (mind blue and red steams in Fig. 6).

To switch from permanent to transient mode or vice versa, the following criterion applies:

$$\mathrm{mode[t]} = \begin{cases} \mathrm{transient}, & \Delta\mathrm{DVGA[t]}= \mathrm{tran\_tresh} \\ \mathrm{permanent}, & \mathrm{median}\{\Delta\mathrm{DVGA[t-3]}\cdots\Delta\mathrm{DVGA[t]}\} \leq \mathrm{perm\_tresh} \end{cases} \tag{12}$$

where heuristically determined *tran_tresh* $= 20$ and *perm_tresh* $= 10$. In order to enable a smooth transition from transient to permanent mode (12) at least four most recent $\Delta DVGA$ need to be determined during the transient mode operation.

Generally, when a change in the coherency occurs, the value of $\Delta DVGA[t]$ will increase over the *tran_tresh*, leading to the transient mode activation. Contrary, during sustained conditions, the medium value of the four most recent $\Delta DVGA[t]$ should drop below the *perm_tresh*. Notably, in case of a profoundly disturbed power system, leading to continuous transient mode activation, one might need to increase the value of α, *tran_tresh*, and *perm_tresh* to decrease the algorithm's sensitivity.

It is important to note that during the algorithm initialization period (transient mode by default) and when the transition from permanent to transient mode occurs (12) the first $\Delta DVGA[t]$ (10) to be used further in the partitioning (see Section II-G) is equal to most recent $DVG[t]$ by setting $\alpha = 0$ in (10). In this way, the partitioning algorithm considers only the most recent coherency indices (6) and neglects any past contributions. This enables full adaptiveness of the proposed algorithm on the new conditions following a significant event.

4) Time Evolution of Slow Coherency Indices: In a multidimensional dataset, a principal component analysis (PCA) dimensionality reduction method identifies principal components (PC) or directions with the most substantial variance in the dataset variables (dimensions) [16]. In this paper, the PCA is performed on the set of past $DVGA \in \mathrm{R}^{1\times \mathrm{L}}$ vectors (10) to analyze the evolution of generator slow coherency indices over time. In other words, it is possible to visually demonstrate the changes in generator slow coherency indices of a power system, observed as variations in the first (dominant) PC (hereinafter referred to as PC1). For illustration, the black colored line in Fig. 6 presents the PC1 of the 37 $DVGA \in R^{1\times \mathrm{L}}$ vectors of the preformed simulation with 45 dimensions in total, where the vertical changes in the black line resemble the shift in the *DVGA* vectors (and related slow coherency indices) in the most dominant direction over time. In the case of Fig. 6, the PC1 exhibits 61.9 % of the total dataset variance.

G. Partition of Generators Into Coherent Groups

In generator coherency identification, a clustering technique is used to partition a set of N generators as nodes $k \in \{1, 2, \ldots, N\}$ into $C = \{c_1, c_2, \ldots, c_K\}$ clusters (K total number of groups), based on a distance matrix, so that $G = \cup_{i=1}^{K} c_i$ and $c_i \cap c_j = \emptyset$, for $i \neq j$ [32]. The main challenge is to partition the generators into robust (over time) and an optimal number of clusters. This paper extends the unsupervised affinity propagation (AP) clustering technique to partition coherent generators into groups [25].

1) AP Clustering: The AP clustering is an exemplar-based technique, which based on the similarity matrix adopts the max-product algorithm on a factor graph to identify set of nodes as clusters' center (exemplars), and partition the remaining nodes into the corresponding clusters [34], [35]. The AP clustering is based on the message passing approach between nodes, which in iterative steps maximizes the following unconstrained optimization problem:

$$\max \mathrm{F(C, S)} := \sum_{\mathrm{i=1}}^{\mathrm{N}} \mathrm{S(i,c_i)} + \sum_{\mathrm{k=1}}^{\mathrm{N}} \delta_{\mathrm{j}}(\mathrm{c}) \forall \mathrm{i, k} \leq \mathrm{N} \qquad (13)$$

where $S(i,c_i)$ denotes the negative dissimilarity matrix between node i and its potential exemplar c_i, and δ_j (C) is a coherence constraint to guarantee the exemplar-consistency and eliminate incorrect results, defined as:

$$\delta_{\mathrm{j}}(\mathrm{C}) = \begin{cases} -\infty, & \text{if } \mathrm{c_j} \neq \mathrm{j}, \text{ but } \exists\ \mathrm{c_i} = \mathrm{j} \\ 0, & \text{otherwise} \end{cases} \qquad (14)$$

To identify K exemplars as cluster centers and partition the remaining nodes into corresponding C clusters, the AP takes the negative distance matrix as an input ($S = -DM \in R^{N\times N}$) and recursively updates the responsibility matrix $R(i, k) = S(i, k) - \max\{A(i, j) + S(i, j)\} \in R^{N\times N}$, where $j \in \{1, 2, \ldots, n\}$ but $j \in k$, representing the accumulated evidence of node k to be the exemplar for node i, and the availability matrix $A(i, k) = min\{0, R(k, k)+sum\{max(0, R(j, k))\}\}$, where $j \in \{1, 2, \ldots, n\}$, but $j \neq i$ and $j \neq k$, representing the accumulated evidence of node k to be the exemplar for node i. Detailed iteration formulas can be found in [34], [35]. Finally, the resulting clusters C can be obtained by:

$$\mathrm{c_i[t]} = \arg\max_{\mathrm{k}}\{\mathrm{A(i, k) + R(i, k)}\}. \qquad (15)$$

2) AP Preferences Parameter: The initialization of AP preference parameter $p = \{p_k\}$, in $S(k, k) = p_k$ plays an important role in AP to facilitate node k to be elected as an exemplar, control the total number of identified clusters, and avoid trivial solution as every node chooses itself as its exemplar. Frey and Dueck suggests p being the median of the input similarity matrix [34]. In many cases, this approach leads to suboptimal clustering results, since it tends to cluster the outlier nodes (often implied as independent exemplars) to the centrally oriented exemplars [25], [35].

In order to overcome this problem, a novel *AP preferences parameter* adaptive method is proposed for the identification of exemplary nodes. The proposed method identifies outlier generators as independent clusters, automatically determines a finite number of groups, and reduces the number of iteration steps of AP clustering to converge. It is based on distribution of values of $DVGA[t]$ distance vector in order to locate cluster exemplars and related cluster sub-nodes. In short, the method first, presumes all nodes as being potential exemplars. Second, based on the similarity matrix of $DVGA[t]$ searches for centrally oriented nodes and marks them as exemplars. Third, based on the combination of mean and median absolute value of $DVGA[t]$ distance vector in multiple steps identifies the cluster sub-nodes and rejects them for being exemplars. Finally, the method returns the defined preference vector p with identified exemplar nodes as:

$$\mathrm{p_k} = \begin{cases} 0, & \text{exemplar} \\ -\infty, & \text{subnode} \end{cases} \qquad (16)$$

The following pseudocode illustrates the implementation procedure of the proposed AP preference adjustment method.

Pseudocode 1 Determination of AP preference *p* parameter

```
input: DVGA[t], output: p
ex = {ex_k} j 1, k ∈ {1,2,..., N} //init: nodes as exemplars
pn j {sn_k} = 0, k ∈ {1,2,..., N}//init: processed nodes
dc = (mean(DVGA) + mad(DVGA)) · β //distance to cut based on DVGA
value distribution
ca = sort(DVGA) //sort in ascending order
DMGA = squareform(DVGA) //convert to N×N matrix
for i = 1 to size(ca) //for each distance of DVGA
  {m, n} = find{DMGA == ca(i)} //find node matrix indexes
  if pn(n) == 0 ∧ ex(n) j 1 ∧ median{DMGA(:,n)} <=
median{DMGA(:,m)}
    ce = n //node n as potential exemplar
    cs = m //node m as potential sub-node
    go = true //flag to continue
  elseif pn(m) == 0 ∧ ex(m) == 1
    ce = m //node m as potential exemplar
    cs = n //node n as potential sub-node
    go = true //flag to continue
  else
    go = false //flag, nothing identified
  endif
  if go //continue with procedure?
    pn(ce) = 1 //mark node as exemplar & processed
    s = find[{DMGA(:,ce) = dc} ∉ ¬ pn] //find nodes as sub-nodes that
are not already processed
    if size(s) > 0 //cluster sub-nodes identified
      ex(s) = 0 //reject sub-nodes as exemplars
      pn(s) = 1 // mark sub-nodes as processed
      for x = 1 to size(s) //for each sub-node
        r = find[{DMGA(:,s(x))≤dc} ∉ ¬ pn] //find more sub-nodes that
are not already processed
        if size(r) > 0 //sub-nodes of cluster sub-nodes
          ex(r) = 0 //reject sub-nodes as exemplars
          pn(r) = 1 //mark sub-nodes as processed
        endif
      endfor
    else
      pn(cs) = 1 //mark node as processed
    endif
  endif
endfor
p = ex − 1 // mark as exampler (16)
p(p == −1) = −Inf // mark as subnode (16)
```

Notably, one can influence the granularity of identified groups by changing the parameter β value. Generally, a higher value of β reflects in a smaller number of groups (stiffer grouping), while a smaller value results in a higher number of groups. Based on the performed simulations, the $\beta = 0.2$ results in the most rational number of identified groups.

H. Proposed Methodology Flowchart

In summary, the proposed algorithm, firstly, preprocesses the incoming PMU frequency measurements with a low-pass filter; secondly, by using the improved distance measure it adaptively determines the minimum number of observation window samples; thirdly, it searches for the interfering coherency indices and retains only the observation window samples containing the most recent coherency indices; fourthly, performs adaptive tracking of grouping changes of slow coherent generators; finally, adaptively identifies a finite number of groups and partitions the coherent generators. Fig. 2 presents the corresponding flowchart of the algorithm.

III. Simulation Platform

In order to demonstrate proposed algorithm capabilities, the cyber-physical simulation platform (see Fig. 3) is utilized as a co-simulation between the SMT supported electric power system model and underlying ICT infrastructure in real-time [36]. For this purpose, the IEEE 39-bus benchmark model is simulated in the RTDS power system digital simulator [37]. The GTNETx2 based PMUs, installed on the generator terminal buses, are of class P with 60 fps reporting rate. The PMU measurements are sent to the SEL-5073 Phasor Data Concentrator (PDC) for aggregation and time-alignment. The aggregated PMU measurements are further sent to a PC running the Synchro-measurement Application Development Framework (SADF) [29], where the proposed coherency identification algorithm and the benchmark method are implemented and executed as an online MATLAB program in real-time. To provide time synchronization between all components, a GE RT430 grandmaster GPS clock is used for IRIG-B and IEEE 1588 Precise Time Protocol based time dissemination.

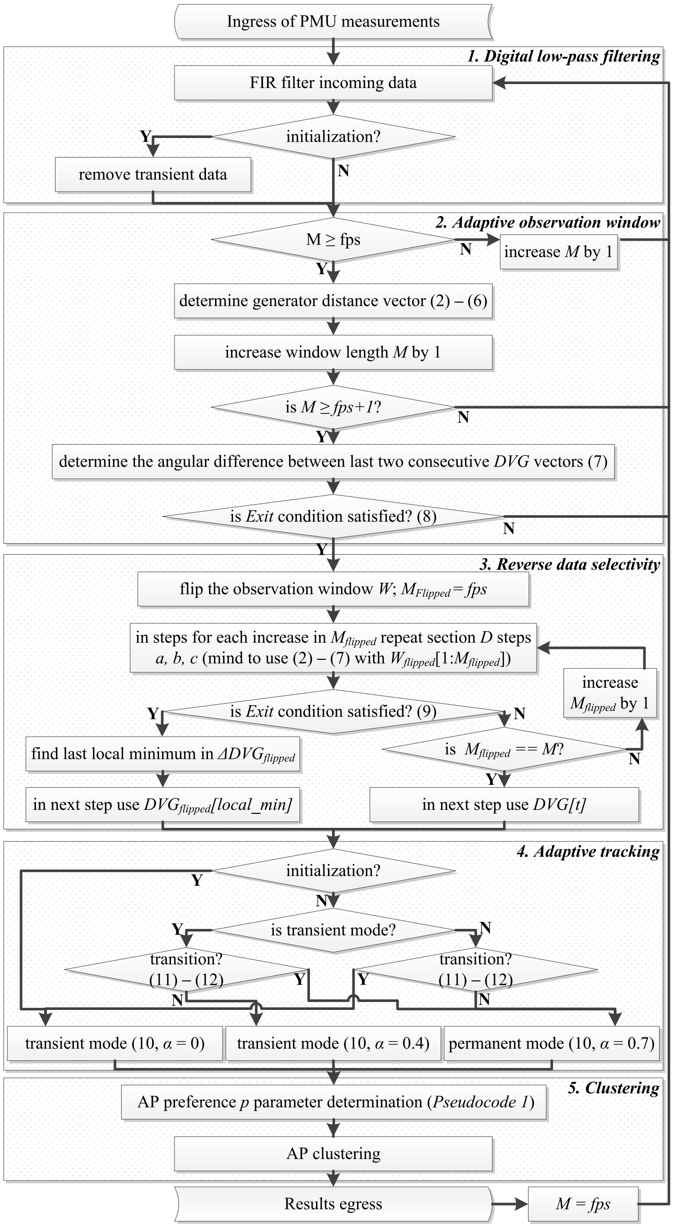
Ingress of PMU measurements
1. Digital low-pass filtering
FIR filter incoming data
initialization?
Y
N
remove transient data
2. Adaptive observation window
M ≥ fps
N
increase M by 1
Y
determine generator distance vector (2) – (6)
increase window length M by 1
is M ≥ fps+1?
N
Y
determine the angular difference between last two consecutive DVG vectors (7)
is Exit condition satisfied? (8)
N
Y
3. Reverse data selectivity
flip the observation window W; M_Flipped = fps
in steps for each increase in M_flipped repeat section D steps a, b, c (mind to use (2) – (7) with W_flipped[1:M_flipped])
increase M_flipped by 1
is Exit condition satisfied? (9)
Y
N
find last local minimum in ΔDVG_flipped
is M_flipped == M?
N
Y
in next step use DVG_flipped[local_min]
in next step use DVG[t]
4. Adaptive tracking
initialization?
Y
N
is transient mode?
Y
N
transition? (11) – (12)
transition? (11) – (12)
N
Y
Y
N
transient mode (10, α = 0)
transient mode (10, α = 0.4)
permanent mode (10, α = 0.7)
5. Clustering
AP preference p parameter determination (Pseudocode 1)
AP clustering
Results egress
M = fps

Fig. 2. Flowchart of the proposed online algorithm.

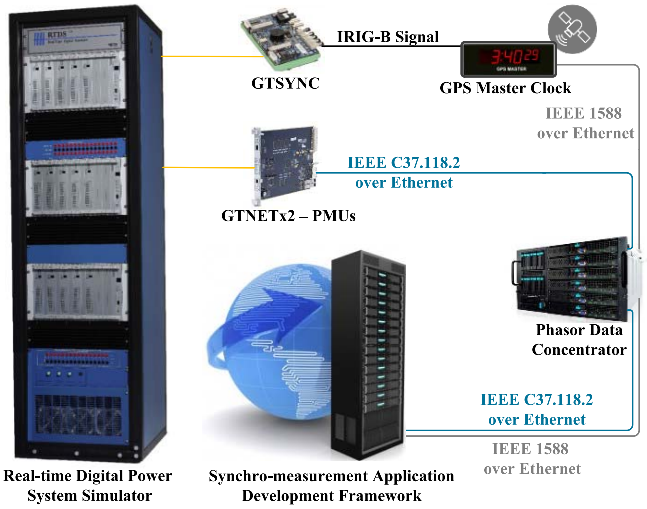

Fig. 3. SMT supported real-time cyber-physical simulation platform.

IV. Simulation Results

This section presents the clustering performance of the proposed algorithm and the benchmark method on the IEEE 39-bus system [1], wherein the generator G1 represents the aggregation of the remaining New England system, being connected to Bus-39. For the sake of clarity, the algorithm performance is demonstrated on a limited set of excited modes. For this purpose, the generator G1 mechanical torque is being modulated every 200 *ms* with a random perturbation within ± 1 % of the nominal value [17].

For result comparison, the benchmark method parameters $\gamma = \gamma_{\mathrm{r}} = 0.9999$ are tuned to achieve the most rational results. However, the benchmark method paper fails to detail the observation window length. To bridge the gap, both methods are compared side-by-side, where the observation window length is online determined by the proposed method. The only differences are that the benchmark method makes use of raw frequency deviation measurements [15].

In all the result figures, the white area marks measurements (raw or processed) that are being used for the analysis; the grey area marks the raw measurements effected by the filtering delay, if applicable; and the red area marks the measurements being discarded due to detected interfering coherency indices of the reverse data selectivity, if applicable.

Unfortunately, the number of presented graphical results is intentionally limited. Nevertheless, readers are encouraged to run the offline simulation available on *Code Ocean* to acquire in total 37 successive graphical results of the following simulated three use-cases, constructing in total 86.6 *s* of simulation and 5197 PMU frequency measurements per generator. It is important to note that the presented results are obtained by executing the following three use-cases successively without interruption of the simulation. Table II presents the clustering results of the comparison for each of 37 coherency identification instances in total, where time in the brackets of the table's first column resembles the simulation time equal to the observation window center of each instance. Table II clustering results in bold indicate an exact result match of the proposed algorithm and the benchmark method.

TABLE II
Results of Simulation

instance (time)	proposed algorithm	benchmark method
1. (2.06 *s*)	{G1} {G2, G3, G8, G10} {G4, G5, G6, G7, G9}	{G1} {G2, G3, G4, G5, G6, G7, G8, G9, G10}
2. (3.75 *s*)	**{G1} {G2, G3, G8, G10} {G4, G5, G6, G7, G9}**	**{G1} {G2, G3, G8, G10} {G4, G5, G6, G7, G9}**
3. (5.03 *s*)	{G1} {G2, G3, G8, G10} {G4, G5, G6, G7, G9}	{G1} {G2, G3, G4, G5, G6, G7, G8, G9, G10}
4. (6.55 *s*)	{G1} {G2, G3, G8, G10} {G4, G5, G6, G7, G9}	{G1} {G2, G3, G4, G5, G6, G7, G8, G9, G10}
5. (8.5 *s*)	**{G1} {G2, G3, G8, G10} {G4, G5, G6, G7, G9}**	**{G1} {G2, G3, G8, G10} {G4, G5, G6, G7, G9}**
6. (10.46 *s*)	{G1} {G2, G3, G8, G10} {G4, G5, G6, G7, G9}	{G1} {G2, G3, G4, G5, G6, G7, G8, G9, G10}
7. (12.43 *s*)	{G1} {G2, G3, G8, G10} {G4, G5, G6, G7, G9}	{G1} {G2, G3, G4, G5, G6, G7, G8, G9, G10}
8. (14.05 *s*)	**{G1} {G2, G3, G8, G10} {G4, G5, G6, G7, G9}**	**{G1} {G2, G3, G8, G10} {G4, G5, G6, G7, G9}**
9. (19.81 *s*)	{G1} {G2, G3, G10} {G4, G5, G6, G7} {G8, G9}	{G1} {G2} {G3} {G4} {G5} {G6, G7} {G8} {G9} {G10}
10. (21.85 *s*)	{G1} {G2, G3, G10} {G4, G5, G6, G7} {G8, G9}	{G1} {G2} {G3} {G4} {G5} {G6, G7} {G8} {G9} {G10}
11. (24.03 *s*)	{G1} {G2, G3, G10} {G4, G5, G6, G7} {G8, G9}	{G1} {G2} {G3} {G4} {G5} {G6, G7} {G8} {G9} {G10}
12. (26.43 *s*)	{G1} {G2, G3, G10} {G4, G5, G6, G7} {G8, G9}	{G1} {G2, G3} {G4, G5, G6, G7} {G8} {G9} {G10}
13. (28.55 *s*)	{G1} {G2, G3, G10} {G4, G5, G6, G7} {G8, G9}	{G1} {G2, G3, G4, G5, G6, G7, G10} {G8, G9}
14. (30.96 *s*)	**{G1} {G2, G3, G10} {G4, G5, G6, G7} {G8, G9}**	**{G1} {G2, G3, G10} {G4, G5, G6, G7} {G8, G9}**
15. (34.18 *s*)	**{G1} {G2, G3, G10} {G4, G5, G6, G7} {G8, G9}**	**{G1} {G2, G3, G10} {G4, G5, G6, G7} {G8, G9}**
16. (37.48 *s*)	{G1} {G2, G3, G10} {G4, G5, G6, G7} {G8, G9}	{G1} {G2, G3, G8, G9, G10} {G4, G5, G6, G7}
17. (40.2 *s*)	{G1} {G2, G3, G10} {G4, G5, G6, G7} {G8, G9}	{G1} {G2, G3, G10} {G4, G5, G6, G7, G8, G9}
18. (42.45 *s*)	**{G1} {G2, G3, G10} {G4, G5, G6, G7} {G8, G9}**	**{G1} {G2, G3, G10} {G4, G5, G6, G7} {G8, G9}**
19. (46.36 *s*)	**{G1} {G2, G3, G10} {G4, G5, G6, G7} {G8, G9}**	**{G1} {G2, G3, G10} {G4, G5, G6, G7} {G8, G9}**
20. (49.81 *s*)	**{G1} {G2, G3, G10} {G4, G5, G6, G7} {G8, G9}**	**{G1} {G2, G3, G10} {G4, G5, G6, G7, G8, G9}**
21. (51.55 *s*)	**{G1} {G2, G3, G10} {G4, G5, G6, G7} {G8, G9}**	**{G1} {G2, G3, G10} {G4, G5, G6, G7} {G8, G9}**
22. (53.43 *s*)	**{G1} {G2, G3, G10} {G4, G5, G6, G7} {G8, G9}**	**{G1} {G2, G3, G10} {G4, G5, G6, G7} {G8, G9}**
23. (57.1 *s*)	{G1} {G2, G3} {G4, G5, G6, G7} {G8, G10} {G9}	{G1} {G2} {G3} {G4} {G5} {G6, G7} {G8} {G9} {G10}
24. (59.01 *s*)	{G1} {G2, G3, G8, G10} {G4, G5, G6, G7} {G9}	{G1} {G2} {G3} {G4} {G5} {G6, G7} {G8} {G9} {G10}
25. (60.98 *s*)	{G1} {G2, G3, G8, G10} {G4, G5, G6, G7} {G9}	{G1} {G2, G3} {G4, G5, G6, G7} {G8, G10} {G9}
26. (62.96 *s*)	{G1} {G2, G3, G8, G10} {G4, G5, G6, G7} {G9}	{G1} {G2, G3, G8, G10} {G4, G5, G6, G7, G9}
27. (65.01 *s*)	{G1} {G2, G3, G8, G10} {G4, G5, G6, G7, G9}	{G1} {G2, G3, G4, G5, G6, G7, G8, G9, G10}
28. (66.65 *s*)	**{G1} {G2, G3, G8, G10} {G4, G5, G6, G7, G9}**	**{G1} {G2, G3, G8, G10} {G4, G5, G6, G7, G9}**
29. (69.18 *s*)	**{G1} {G2, G3, G8, G10} {G4, G5, G6, G7, G9}**	**{G1} {G2, G3, G8, G10} {G4, G5, G6, G7, G9}**
30. (71.75 *s*)	**{G1} {G2, G3, G8, G10} {G4, G5, G6, G7, G9}**	**{G1} {G2, G3, G8, G10} {G4, G5, G6, G7, G9}**
31. (74.11 *s*)	{G1} {G2, G3, G8, G10} {G4, G5, G6, G7, G9}	{G1} {G2, G3, G4, G5, G6, G7, G8, G9, G10}
32. (76.31 *s*)	**{G1} {G2, G3, G8, G10} {G4, G5, G6, G7, G9}**	**{G1} {G2, G3, G8, G10} {G4, G5, G6, G7, G9}**
33. (78.43 *s*)	{G1} {G2, G3, G8, G10} {G4, G5, G6, G7, G9}	{G1} {G2} {G3} {G4} {G5} {G6} {G7} {G8} {G9} {G10}
34. (80.53 *s*)	{G1} {G2, G3, G8, G10} {G4, G5, G6, G7, G9}	{G1} {G2} {G3} {G4} {G5} {G6, G7} {G8} {G9} {G10}
35. (81.78 *s*)	{G1} {G2, G3, G8, G10} {G4, G5, G6, G7, G9}	{G1} {G2} {G3} {G4} {G5} {G6, G7} {G8} {G9} {G10}
36. (83.18 *s*)	{G1} {G2, G3, G8, G10} {G4, G5, G6, G7, G9}	{G1} {G2} {G3} {G4} {G5} {G6, G7} {G8} {G9} {G10}
37. (84.56 *s*)	{G1} {G2, G3, G8, G10} {G4, G5, G6, G7, G9}	{G1} {G2, G3, G8, G10} {G4, G5, G6, G7} {G9}

A. *Quasi-Steady-State Operation*

During quasi-steady-state operation (see Fig. 4 and Fig. 5 - top, displaying results of the 7th instance in Table II) the proposed algorithm identifies three groups of coherent generators as $c_1 = \{G1\}$, $c_2 = \{G2, G3, G8, G10\}$, and

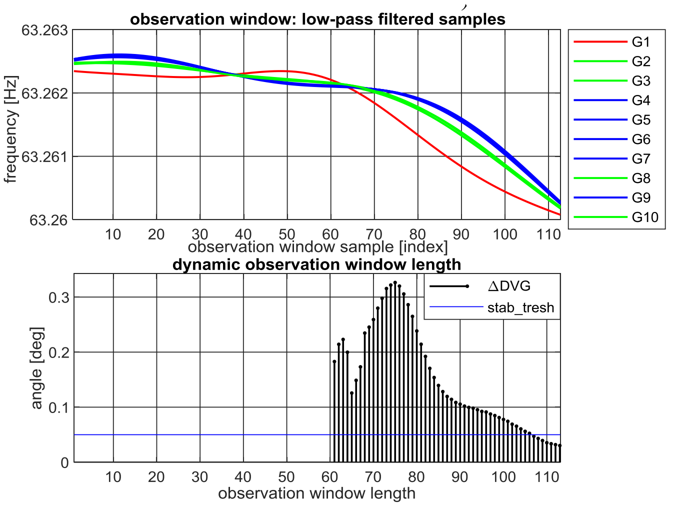

Fig. 4. Visualized procedure to determine the observation window length (bottom); and corresponding low-pass filtered frequency measurements, colored according to the identified groups of slow coherent generators (top).

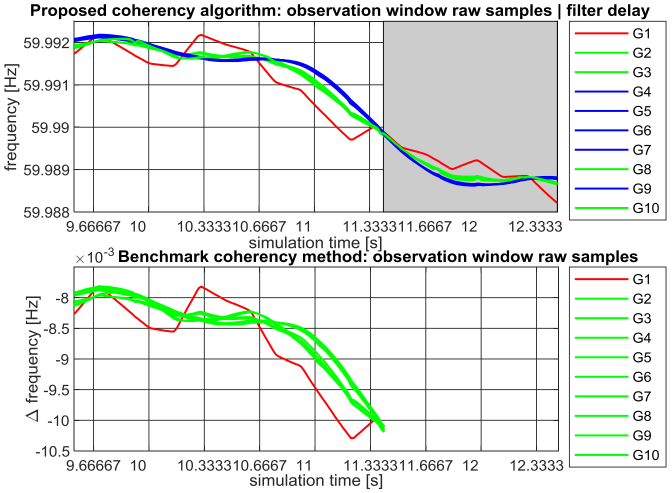

Fig. 5. Quasi-steady-state; the proposed algorithm identifies three groups (top); while the benchmark method identifies two groups (bottom).

$c_3 = \{G4, G5, G6, G7, G9\}$ continuously (mind the orange area in Table II between 1st and 8th instance).

Moreover, in Fig. 6 the PC1 on the past *DVGAs* shows no significant deviations (mind the black colored line from 1 to 8 in x-axis), indicating sustained generator slow coherency configuration. This behavior is expected and is in accordance with the slow coherency theory [12].

On the other hand, the benchmark method identifies the same three groups as the proposed method and additionally two coherent groups as $c_1 = \{G1\}$, $c_2 = \{G2, G3, G4, G5, G6, G7, G8, G9, G10\}$ interchangeably (see Table II). For example, as seen in Fig. 5 - bottom, the benchmark algorithm is affected by the mechanical torque modulation of the generator G1 leading to unstable results despite the quasi-sustained state.

B. Applied Three-Phase Self-Cleared Fault on Bus B25 With Permanent Tripping of Line B2-B25 and Delayed Reconnection

Following use-case A (mind the blue area in Table II between 9th and 22nd instance), first in use-case B, a three-phase 80 *ms* fault is applied on bus B25 at 18.3 *s* of the simulation leading to permanent disconnection of the line B2-B25. The system perturbation following the event can be observed in Fig. 7 - top and Fig. 8.

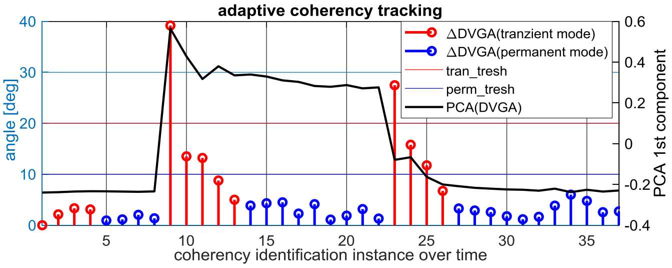

Fig. 6. Coherency tracking progress of the preformed simulation, where the increase in angular deviation of two successive *DVGA* over the *tran_tresh* indicates a significant change in coherency following a disturbance. The red stems present transient mode coherency identification instances, while the blue stems present permanent mode coherency identification instances. The black line presents the PC1 of the past *DVGA*s.

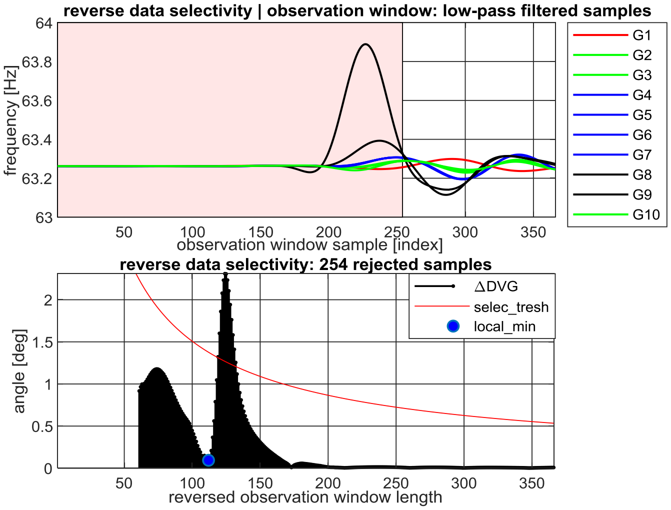

Fig. 7. Detected interfering pre- and post-event coherency indices after the topology change (bottom); and the corresponding low-pass filtered frequency measurements (top). The red area marks the rejected pre-event measurements.

To clarify, the line disconnection changes the power system topology, which also affects the generator coherency. In this case, as indicated in Fig. 7 - bottom, the proposed reverse data selectivity method identifies the interfering pre- and post-event coherency indices in the given observation window (mind the intersection between the black stems and red line in Fig. 7 - bottom). In the next step, the method also identifies the transition point (mind the blue dot in Fig. 7 - bottom) and discards the pre-event measurements (mind the red area in Fig. 7 - top). In this way, only the post-event coherency indices are taken into account for further processing.

The change in generator coherency, caused by the topology change, can also be observed in Fig. 6 as a jump in the PC1 (mind the black colored line and its vertical increase from 8 to 9 in x-axis). Herby, an increase in ΔDVGA [9] above the *tran_tresh* triggers the activation of the transient mode for the following five coherency estimation instances (mind the red steams from 9 to 13 in x-axis). Afterward, the adaptive tracking method switches back to permanent mode due to the

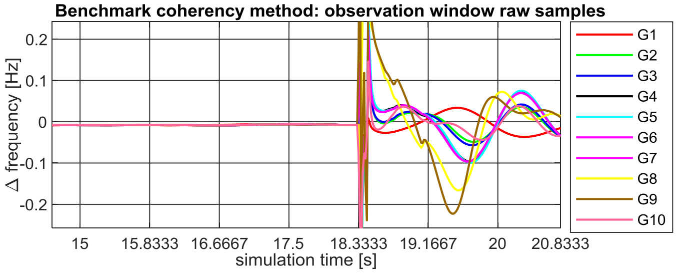

Fig. 8. Applied fault resulting in the permanent line trip, where the benchmark method identifies nine groups of coherent generators (mind the legend colors).

new quasi-steady-state conditions (mind the blue steams from 14 to 22 in x-axis in Fig. 6).

As seen in Fig. 6, the PC1 gradually stabilize in new value after the initial jump indicating new quasi-sustained conditions and corresponding coherency configuration (mind the relatively narrow section of the black colored line between 9 and 22 in x-axis). Immediately after the fault and line disconnection (see Fig. 7 - top), the proposed algorithm identifies new four coherent groups as $c_1 = \{G1\}$, $c_2 = \{G2, G3, G10\}$, $c_3 = \{G4, G5, G6, G7\}$, and $c_4 = \{G8, G9\}$ continuously. Compared to the use-case A (pre-event), the generator G8 of group c_2 and G9 of group c_3 split from their existing groups (mind Fig. 4 - top) and form a new independent group c_4 as a result of the topology change following the line disconnection.

On the contrary, the benchmark method identifies nine coherent groups with only generator G6 and generator G7 belonging to the same coherent group (see Fig. 8 and Table II). Similar occurs following five times (taking $\sim$11 *s*) after the fault before it matches the results of the proposed algorithm. Yet, the benchmark method continues to produce variable results, while on the contrary, the proposed algorithm continuously identifies precisely the same groups as immediately after the line disconnection.

Following 37 *s* of the simulation after the initial fault, the B2-B25 line is reconnected, leading back to the same topology as in use-case A (mind the red area in Table II between 23rd and 32nd instance). Herby, the proposed algorithm first identifies five groups of coherent generators (see Fig. 9 - top) as $c_1 = \{G1\}$, $c_2 = \{G2, G3\}$, $c_3 = \{G4, G5, G6, G7\}$, $c_4 = \{G8, G10\}$, and $c_5 = \{G9\}$. This moment can be observed in Fig. 6 at ΔDVGA [23] when the tracking algorithm switches to transient mode due to the line reconnection. Also, in this use-case, the proposed algorithm identifies the interfering coherency indices due to the topology change (see Fig. 9 - bottom). In the next three coherency identification instances, the proposed algorithm identifies four groups of coherent generators (see Fig. 9 - top) as $c_1 = \{G1\}$, $c_2 = \{G2, G3, G8, G10\}$, $c_4 = \{G4, G5, G6, G7\}$, $c_4 = \{G9\}$. Afterward, the proposed algorithm starts to identify the same groups as in use-case A, as a response of the generator G9 resynchronization with the group c_3. This moment is seen in Fig. 6, where the PC1 drops in steps and stabilize near its initial value of use-case A (mind the relatively narrow section of the black colored line between 23 and 32 in x-axis).

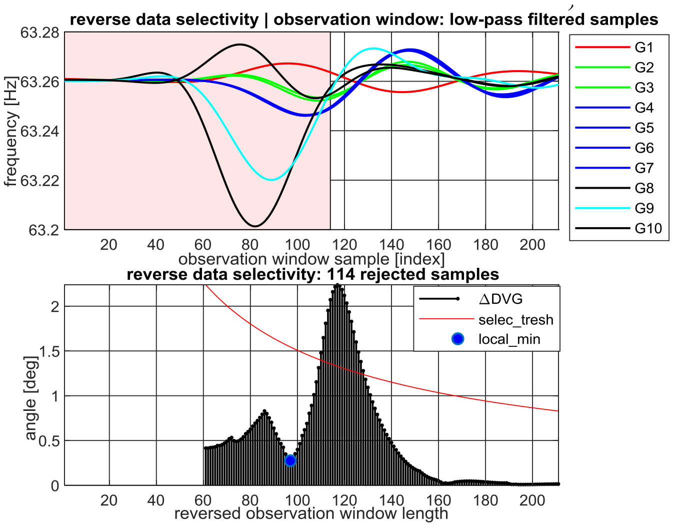

Fig. 9. Detected interfering pre- and post-event coherency indices after the line reconnection (bottom); and corresponding low-pass filtered frequency measurements (top). The red area marks the rejected pre-event measurements.

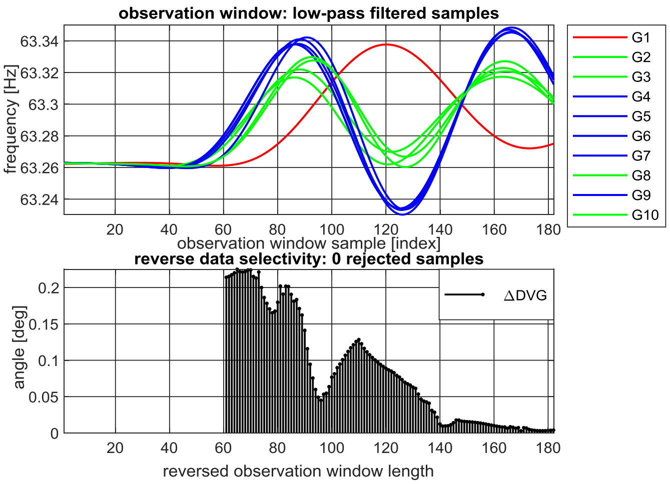

Fig. 10. Continuously identified three coherent generator groups before and after the three-phase self-cleared fault (top); and corresponding reverse data selectivity (bottom) indicating no major coherency change after the event.

On the other hand, after the line reconnection, the benchmark method first identifies the same nine groups as when the line B2-B25 is disconnected followed by producing variable results in time as seen in Table II (mind the red area). After five instances, the benchmark method matches with the results of the proposed algorithm.

C. Three-Phase Self-Cleared Fault on Bus B14

In this example (mind the green area in Table II between 33rd and 37th instance), quasi-steady-state conditions as in the use-case A, are followed by a three-phase 80 *ms* self-cleared fault on bus B14 at 78.1 *s* of the simulation leading to the system perturbation as seen in Fig. 10 - top.

As seen in Fig. 6 at $\Delta DVGA$ [33] and in PC1 (mind the narrow section of the black colored line between 33 and 37 in x-axis), the slow coherency indices do not change significantly after the fault. This leads that the proposed algorithm continuously identifies the same groups of slow coherent generators $c_1 = \{G1\}$, $c_2 = \{G2, G3, G8, G10\}$, and $c_3 = \{G4, G5, G6,$

G7, G9} exactly as in the use-case A and use-case B after the line reconnection. To clarify, the applied temporal fault does not affect the system structure permanently, leading to sustained slow coherency identification before and after the fault. This behavior is expected and is in accordance with the slow coherency theory [12]. On the contrary, the benchmark method is significantly affected by the temporary fault perturbation resulting in identified nine coherent groups with only generator G6 and generator G7 belonging to the same group, following the variable results over time.

V. Discussion

A. Comparison With the Benchmark Method

The result comparison suggests that the proposed algorithm overcomes the limitations of the benchmark method for the purpose of ICI. In particular, the low-pass filtering of measurements (addressed in Section II-B) of the proposed algorithm enables identification of slow coherent generator groups based on the superposition of the crucial inter-area oscillation modes only, while the benchmark method uses raw measurements containing higher frequency local modes and transients. As shown, the improved similarity method (addressed in Section II-C) can assess the coherency indices in greater detail, leading to more sustained results and identification of slow coherent areas with different frequency, while the benchmark method cannot distinguish different frequency zones (mind Fig. 5). Especially, after a significant disturbance leading to the change in slow coherency, the proposed reverse data selectivity (addressed in Section II-E) prevents mixing of interfering pre- and post-event coherency indices and retains only the measurements belonging to the post-event for more reliable results, while the benchmark method does not take that into account. The adaptive observation window length method (addressed in Section II-D) identifies the minimum number of processed samples for fast identification of generator slow coherent groups following a contingency, while the benchmark method uses a fixed observation window length. The proposed adaptive tracking method (addressed in Section II-F) of grouping changes of slow coherent generators during the quasi-steady-state and electromechanical transient period following a disturbance, makes the results more robust to temporal changes in coherency, but still permits adaptiveness of results in case of significant disturbances. On the contrary, the benchmark method does not perform adaptive tracking and produces results based on the identified most recent coherency indices, leading to altering results even during quasi-sustained power system state. Finally, the fixed clustering parameter $\gamma_c = \gamma_r$ in the benchmark method leads to the high number of identified clusters following a disturbance, while the proposed AP preference parameter method can dynamically adapt to the present conditions (addressed in Section II-G) leading to sustained and more robust results. As shown in Fig. 6, the applied PCA enables unprecedented visual demonstration of changes in generator slow coherency indices over time.

B. Proposed Algorithm's Requirements and Performance

This paper assumes that each generator unit is observed by a PMU installed at its terminal. However, in case of the limited generator observability in practice, one could use a single PMU to monitor the behavior of a generation region of electrically-short-connected slow coherent generators, such as large power plants. But beforehand, a comprehensive dynamic equivalencing analysis of the detailed power system model should be performed.

Moreover, 60 fps PMU reporting rate is used for the analysis, while in practice 30 fps or less might be available only. Nevertheless, the preformed simulations (not part of this paper) confirm that the proposed algorithm performance is not affected in case of used 10, 15, or 30 fps PMU reporting rate. The readers are encouraged to run the offline simulation available on Code Ocean to obtain the corresponding results.

As observed in Fig. 4, Fig. 7, Fig. 9 and Fig. 10, the amplitudes of frequency measurements are altered as a side effect of the applied low-pass FIR filtering beforehand. This has no adverse effect on the results of the proposed algorithm.

During the simulation of all three use-cases (37 coherency identifications in total), a median observation window length of 113 samples (1.933 s) with 52 samples of standard deviation is determined automatically. It takes 0.36 ms execution time to process 950 samples of the median observation window (mind ten generators). After (8) is satisfied, it takes an additional 24.2 ms to perform reverse data selectivity, tracking, and generator clustering, while the benchmark method requires only 1.5 ms in total. To summarize, the average coherency identification latency τ_{total} can be defined as:

$$\begin{aligned}\tau_{\text{total}} &= \tau_{\text{PMU}} + \tau_{\text{comm}} + \tau_{\text{PDC}} + \tau_{\text{SADF}} + \tau_{\text{filt}} + \tau_{\text{win}} + \tau_{\text{proc}} \\ &\approx 21\ ms + 1\ ms + 0.6\ ms + 1.5\ ms + 1.05\ s + 0.96\ s \\ &\quad + 24.3\ ms = 2.05\ s \end{aligned} \tag{17}$$

where τ_{PMU} is the PMU measurement estimation delay; τ_{comm} is the delay between the PMU, PDC, and SADF; τ_{PDC} is the PDC processing delay; τ_{SADF} is SADF parsing delay of the PMU measurements; τ_{filt} is the low-pass filter delay; τ_{win} is the delay of an observation window center ($M/2$); and τ_{proc} is the proposed algorithm processing delay. As observed in (17), the unavoidable low-pass filtering and observation window length are the most significant factors contributing to the overall latency. Still, this mostly outperforms the existing methods due to the relatively short observation window used.

Due to hardware limitations of the RTDS infrastructure it is not possible to verify the performance of the algorithm on a large network with several hundred busses. Instead, the required execution time of the proposed AP preference p parameter method together with the AP clustering is evaluated for different number of nodes (PMU observed generators). For this, the median execution time of 100 iterations of randomly generated distance matrices concerning the increasing number of nodes to partition is compared. Hereby, the AP clustering automatically stops when the results of the last 20 iterations converge. The following Table III presents the obtained results. It can be observed that the required execution time to cluster the nodes exponentially increases with the increasing number of nodes.

In summary, the adverse coherency identification latency, particularly affecting the supported closed-loop control applications, depends on many case dependent factors. Notably, one should consider delays associated with the PMU

TABLE III
AP PREFERENCE p AND CLUSTERING EXECUTION TIME

number of nodes	execution time [s]	number of nodes	execution time [s]
10	0.0028	160	0.2867
20	0.0041	180	0.4152
40	0.0087	200	0.5880
60	0.0180	220	0.8045
80	0.0345	240	1.0631
100	0.0634	260	1.4204
120	0.1076	280	1.8426
140	0.1863	300	2.3729

measurement, remote data acquisition, PDC time-aligning, coherency identification, application's processing, and final control signal conveying to remote actuators. It is important to carefully assess to overall latency to assure the adequate response of mission-critical applications in time.

VI. CONCLUSION

This paper presents a novel SMT supported algorithm for an online and near real-time tracking of grouping changes of the slow coherent generators in an interconnected power system. The proposed algorithm identifies groups of slow coherent generators based on the superposition of the inter-area oscillation modes during the quasi-steady-state and electromechanical transient period following a disturbance. The algorithm, for the first time, detects and removes the interfering pre-event measurements in an observation window and adaptively tracks grouping changes of slow coherent generators, leading to improved accuracy and more robust results, respectively. Moreover, the improved similarity method leads to the identification of areas with different frequency; meanwhile the new AP preference adjustment method adaptively determines the optimal number of slow coherent groups and partitions the outlier generators as independent clusters. All together in combination with the novel adaptive observation window method, which determines the minimum number of samples to be processed for near real-time coherency identification, facilitates the design of fast-acting and adaptive SIPS, such as ICI.

Finally, for ease of the result reproducibility, the MATLAB implementation of the proposed algorithm and the simulation dataset are available as an open-source on Code Ocean platform. At present, the research team is focusing on the development of closed-loop coordinated ICI. Future work is considered to isolate the dominant interarea mode in an interconnected power system and partition the generators accordingly. Also, it is required to verify the proposed algorithm on larger power system networks with several hundred busses.

ACKNOWLEDGMENT

The authors very gratefully acknowledge the in-kind contributions of GE and SEL by the means of hardware and software, respectively.

REFERENCES

[1] M. Liserre, T. Sauter, and J. Y. Hung, "Future energy systems: Integrating renewable energy sources into the smart power grid through industrial electronics," *IEEE Ind. Electron. Mag.*, vol. 4, no. 1, pp. 18–37, Mar. 2010.

[2] G. Andersson *et al.*, "Causes of the 2003 major grid blackouts in North America and Europe, and recommended means to improve system dynamic performance," *IEEE Trans. Power Syst.*, vol. 20, no. 4, pp. 1922–1928, Nov. 2005.

[3] V. Madani *et al.*, "IEEE PSRC report on global industry experiences with system integrity protection schemes (SIPS)," *IEEE Trans. Power Del.*, vol. 25, no. 4, pp. 2143–2155, Oct. 2010.

[4] F. Aminifar, M. Fotuhi-Firuzabad, A. Safdarian, A. Davoudi, and M. Shahidehpour, "Synchrophasor measurement technology in power systems: Panorama and state-of-the-art," *IEEE Access*, vol. 2, pp. 1607–1628, 2014.

[5] V. Terzija *et al.*, "Wide-area monitoring, protection, and control of future electric power networks," *Proc. IEEE*, vol. 99, no. 1, pp. 80–93, Jan. 2011.

[6] M. M. Begovic, *Electrical Transmission Systems and Smart Grids, Introduction*. New York, NY, USA: Springer, Nov. 2012.

[7] H. You, V. Vittal, and X. Wang, "Slow coherency-based islanding," *IEEE Trans. Power Syst.*, vol. 19, no. 1, pp. 483–491, Feb. 2004.

[8] I. Tyuryukanov, M. Naglic, M. Popov, and M. A. M. M. van der Meijden, "Implementation of slow coherency based controlled islanding using digsilent powerfactory and MATLAB," in *Advanced Smart Grid Functionalities Based on PowerFactory* (Green Energy and Technology), F. Gonzalez-Longatt and J. R. Torres, Eds. Cham, Switzerland: Springer, 2018.

[9] L. Ding, Y. Guo, P. Wall, K. Sun, and V. Terzija, "Identifying the timing of controlled islanding using a controlling UEP based method," *IEEE Trans. Power Syst.*, vol. 33, no. 6, pp. 5913–5922, Nov. 2018.

[10] B. P. Padhy, S. C. Srivastava, and N. K. Verma, "A coherency-based approach for signal selection for wide area stabilizing control in power systems," *IEEE Syst. J.*, vol. 7, no. 4, pp. 807–816, Dec. 2013.

[11] R. Podmore, "Identification of coherent generators for dynamic equivalents," *IEEE Trans. Power App. Syst.*, vol. PAS-97, no. 4, pp. 1344–1354, Jul. 1978.

[12] J. H. Chow, *Power System Coherency and Model Reduction*. New York, NY, USA: Springer, 2013.

[13] M. Klein, G. J. Rogers, and P. Kundur, "A fundamental study of inter-area oscillations in power systems," *IEEE Trans. Power Syst.*, vol. 6, no. 3, pp. 914–921, Aug. 1991.

[14] R. Singh, M. Elizondo, and S. Lu, "A review of dynamic generator reduction methods for transient stability studies," in *Proc. IEEE Power Energy Soc. General Meeting*, 2011, pp. 1–8.

[15] A. M. Khalil and R. Iravani, "A dynamic coherency identification method based on frequency deviation signals," *IEEE Trans. Power Syst.*, vol. 31, no. 3, pp. 1779–1787, May 2016.

[16] M. A. M. Ariff and B. C. Pal, "Coherency identification in interconnected power system—An independent component analysis approach," *IEEE Trans. Power Syst.*, vol. 28, no. 2, pp. 1747–1755, May 2013.

[17] Y. Li, D. Yang, F. Liu, Y. Cao, and C. Rehtanz, "Theoretical foundation of low-frequency oscillations," in *Interconnected Power Systems*. Berlin, Germany: Springer, 2016.

[18] M. Jonsson, M. Begovic, and J. Daalder, "A new method suitable for real-time generator coherency determination," *IEEE Trans. Power Syst.*, vol. 19, no. 3, pp. 1473–1482, Aug. 2004.

[19] D. J. Trudnowski and J. W. Pierre, "Overview of algorithms for estimating swing modes from measured responses," in *Proc. IEEE Power Energy Soc. Gen. Meeting*, Jul. 2009, pp. 1–8.

[20] N. Senroy, "Generator coherency using the Hilbert–Huang transform," *IEEE Trans. Power Syst.*, vol. 23, no. 4, pp. 1701–1708, Nov. 2008.

[21] F. Raak, Y. Susuki, and T. Hikihara, "Data-driven partitioning of power networks via Koopman mode analysis," *IEEE Trans. Power Syst.*, vol. 31, no. 4, pp. 2799–2808, Jul. 2016.

[22] A. Vahidnia, G. Ledwich, E. Palmer, and A. Ghosh, "Generator coherency and area detection in large power systems," *IET Gener. Transm. Distrib.*, vol. 6, no. 9, pp. 874–883, Sep. 2012.

[23] T. Guo and J. V. Milanović, "Online identification of power system dynamic signature using PMU measurements and data mining," *IEEE Trans. Power Syst.*, vol. 31, no. 3, pp. 1760–1768, May 2016.

[24] Z. Lin, F. Wen, Y. Ding, and Y. Xue, "Data-driven coherency identification for generators based on spectral clustering," *IEEE Trans. Ind. Informat.*, vol. 14, no. 3, pp. 1275–1285, Mar. 2018.

[25] Z. Lin *et al.*, "WAMS-based coherency detection for situational awareness in power systems with renewables," *IEEE Trans. Power Syst.*, vol. 33, no. 5, pp. 5410–5426, Sep. 2018.

[26] A. M. Khalil and R. Iravani, "Power system coherency identification under high depth of penetration of wind power," *IEEE Trans. Power Syst.*, vol. 33, no. 5, pp. 5401–5409, Sep. 2018.

[27] D. J. Trudnowski, "Estimating electromechanical mode shape from synchrophasor measurements," *IEEE Trans. Power Syst.*, vol. 23, no. 3, pp. 1188–1195, Aug. 2008.

[28] P. V. Kokotovic, B. Avramovic, J. H. Chow, and J. R. Winkelman, "Coherency based decomposition and aggregation," *Automatica*, vol. 18, no. 1, pp. 47–56, 1982.

[29] M. Naglic, M. Popov, M. A. M. M. van der Meijden, and V. Terzija, "Synchro-measurement application development framework: An IEEE standard C37.118.2-2011 supported MATLAB library," *IEEE Trans. Instrum. Meas.*, vol. 67, no. 8, pp. 1804–1814, Aug. 2018.

[30] L. Vanfretti, S. Bengtsson, and J. O. Gjerde, "Preprocessing synchronized phasor measurement data for spectral analysis of electromechanical oscillations in the nordic grid," *Int. Trans. Elect. Energy Syst.*, vol. 25, no. 2, pp. 348–358, 2015.

[31] D. Macii, D. Fontanelli, G. Barchi, and D. Petri, "Impact of acquisition wideband noise on synchrophasor measurements: A design perspective," *IEEE Trans. Instrum. Meas.*, vol. 65, no. 10, pp. 2244–2253, Oct. 2016.

[32] S. Aghabozorgi, A. S. Shirkhorshidi, and T. Y. Wah, "Time-series clustering—A decade review," *Inf. Syst.*, vol. 53, pp. 16–38, Oct./Nov. 2015.

[33] D. Francois, V. Wertz, and M. Verleysen, "The concentration of fractional distances," *IEEE Trans. Knowl. Data Eng.*, vol. 19, no. 7, pp. 873–886, Jul. 2007.

[34] B. J. Frey and D. Dueck, "Clustering by passing messages between data points," *Science*, vol. 315, no. 5814, pp. 972–976, 2007.

[35] P. Li, H. Ji, B. Wang, Z. Huang, and H. Li, "Adjustable preference affinity propagation clustering," *Pattern Recognit. Lett.*, vol. 85, pp. 72–78, Jan. 2017.

[36] M. Naglic, I. Tyuryukanov, M. Popov, M. van der Meijden, and V. Terzija, "WAMPAC-ready platform for online evaluation of corrective control algorithms," in *Proc. Mediterr. Conf. Power Gener. Transm. Distrib. Energy Convers. (MedPower)*, Belgrade, Serbia, Nov. 2016, pp. 1–6.

[37] *RSCAD 5.003 Manuals: Real-Time Simulation Model of IEEE 39-Bus Power System*, RTDS, Winnipeg, MB, Canada, 2018.

Matija Naglic (Student Member, IEEE) received the Uni.Dipl.Ing. degree in electrical engineering from the Faculty of Electrical Engineering, University of Ljubljana, Ljubljana, Slovenia, in 2012.

He was a Researcher with the Milan Vidmar Electric Power Research Institute, Ljubljana. He is currently a Doctoral Researcher with the Intelligent Electrical Power Grids Group, Delft University of Technology, Delft, The Netherlands. His research interests include real-time monitoring and control of large-scale power systems.

Marjan Popov (Senior Member, IEEE) received the Dipl.-Ing. degree from the University of Skopje, Skopje, Macedonia, in 1993, and the Ph.D. degree in electrical power engineering from the Delft University of Technology, Delft, The Netherlands, in 2002.

In 1997, he was an Academic Visitor with the ARC Research Group, University of Liverpool, Liverpool, U.K., where he was involved in modeling SF6 circuit breakers. His current research interests include future power systems, large-scale power system transients, intelligent protection for future power systems, and wide-area monitoring and protection.

Prof. Popov was a recipient of the IEEE PES Prize Paper Award and the IEEE Switchgear Committee Award in 2011. He has actively participated in WG C4.502 and WG A2/C4.39. He is an Associate Editor of the *International Journal of Electric Power and Energy Systems*. He is a member of CIGRE.

Mart A. M. M. van der Meijden (Member, IEEE) received the M.Sc. degree (*cum laude*) in electrical engineering from the Eindhoven University of Technology, Eindhoven, The Netherlands, in 1981.

He is leading research programs on intelligent electrical power grids, reliable, and large-scale integration of renewable (wind and solar) energy sources in the European electrical power systems and advanced grid concepts. He has more than 30 years of working experience in the field of process automation and the transmission and the distribution of gas, district heating, and electricity. Since 2003, he has been with TenneT TSO, Arnhem, The Netherlands, Europe's first cross-border grid operator for electricity, where he is a Manager of Research and Development/Innovation and was responsible for the development of the TenneT long-term vision on the electrical transmission system. He has been a Full Professor (part-time) with the Department of Electrical Sustainable Energy, Faculty of Electrical Engineering, Mathematics and Computers Science, Delft University of Technology, Delft, The Netherlands, since 2011. His current research interest include large-scale sustainable power systems.

Prof. van der Meijden has joined and chaired different national and international expert groups. He is a member of ENTSO-E/RDIC and CIGRE.

Vladimir Terzija (Fellow, IEEE) was born in Donji Baraci (formerly, Yugoslavia), Bosnia and Herzegovina. He received the Dipl.-Ing., M.Sc., and Ph.D. degrees in electrical engineering from the University of Belgrade, Belgrade, Serbia, in 1988, 1993, and 1997, respectively.

Since 2006, ha has been the Engineering and Physical Science Research Council Chair Professor of power system engineering with the School of Electrical and Electronic Engineering, University of Manchester, Manchester, U.K. From 1997 to 1999, he was an Assistant Professor with the University of Belgrade, Belgrade, Serbia. From 2000 to 2006, he was a Senior Specialist for switchgear and distribution automation with ABB, Ratingen, Germany. Since 2018, he has been a National Thousand Talents Distinguished Professor with Shandong University, China. His current research interests include smart grid applications; wide-area monitoring, protection, and control; multienergy systems; switchgear and transient processes; ICT, data analytics, and digital signal processing applications in power systems.

Prof. Terzija is the recipient of the National Friendship Award, China in 2019. He is an Editor-in-Chief of the *International Journal of Electrical Power and Energy Systems*. He is an Alexander von Humboldt Fellow, a DAAD and Taishan Scholar.